19th WORLD CONFERENCE OF THE ASSOCIATED RESEARCH CENTRES FOR THE URBAN UNDERGROUND SPACE
Belgrade, Serbia, November 4-7, 2025.

ACUUS BELGRADE 2025

Paper No: 3.11.162
DOI: 10.46793/ACUUS2025.3.11.162

HYDROGEOLOGICAL INVESTIGATION AND MONITORING ANALYSIS OF WATER-RELATED HAZARDS IN OPERATIONAL HIGHWAY TUNNELS IN WATER-RICH REGIONS

Yubo Luo[1], Junsheng Yang[2], Qi He[3], Zhiheng Zhu[4], Youcai Tan[5]

Abstract: Water-related hazards frequently occur in operational highway tunnels in Guangdong Province, China, posing significant risks to tunnel safety and stability. This study combines hydrogeological investigations with an analysis of 36 documented cases from six tunnels in the region. The key characteristics examined include hazard depth and location within the tunnel, surrounding rock lithology, hazard manifestations, rock mass quality, preferential seepage pathways, and surface topography, all of which were evaluated for their influence on hazard occurrence. In the Dayaoshan No. 1 Tunnel, monitoring instruments were installed to obtain six months of continuous rainfall and water pressure data, which facilitated an investigation of their correlations. The findings indicate that poor rock mass quality, intense rock weathering, concentrated heavy rainfall, runoff-converging topography, and subsurface preferential seepage pathways are critical contributors to water-related hazards in tunnels. The water pressure response to rainfall demonstrates both temporal lag and spatial variability, with a lag time of approximately 3–7days in this case. Moreover, drainage blockages were found to sustain elevated water pressure levels. Based on the case study, the formation of tunnel water-related hazards can be generalized into three sequential stages: (1) continuous heavy rainfall induces rapid infiltration through preferential pathways; (2) drainage system failure maintains high water pressure; and (3) prolonged high water pressure ultimately leads to structural damage.

Keywords: water-related hazards, operational highway tunnels, rainfall–water pressure monitoring, hydrogeological investigation

1. INTRODUCTION

Operational highway tunnels in water-rich regions are highly susceptible to water-related hazards, particularly in areas characterized by abundant groundwater resources and karst topography. Intense rainfall often induces abrupt increases in groundwater pressure, seepage, and even sudden water inrush events (Li et al., 2015; Wang et al., 2019), posing substantial challenges to both tunnel safety and long-term maintenance(Wu et al., 2024). These risks are further aggravated during the summer rainy season, when extreme precipitation can raise groundwater pressures by several hundred kilopascals within just a few days (Li et al., 2023; Lin et al., 2019). Under such circumstances, tunnel operations may be disrupted, maintenance costs escalate sharply, and failures can result in not only severe economic losses but also major safety threats (Wang et al., 2022; Zhang et al., 2024).

Previous studies have attempted to classify water-related hazards in tunnels. For example, categorized water and mud inrush disasters into three types: karst-related, fault-related, and others (Li et al., 2018). Karst-related hazards involve dissolution fractures, caves, conduits, and underground rivers. Fault-related hazards include water-rich faults, water-conducting faults, and water-blocking faults. Other causes are associated with intrusion contacts, interlayer fractures, and differential weathering.

[1] PhD student, Yubo Luo, Central South University, No. 932 Lushan South Road, Changsha, China, luo.yubo@csu.edu.cn
[2] Professor, Junsheng Yang, PhD, Central South University, No. 932 Lushan South Road, Changsha, China, jsyang@csu.edu.cn
[3] PhD student, Qi He, Central South University, No. 932 Lushan South Road, Changsha, China, 254801041@csu.edu.cn.
[4] Senior Engineer, Zhiheng Zhu, PhD, Guangdong Hualu Transportation Technology Co., Ltd., No. 399 Congyun Road, Guangzhou, China, zzh8207@163.com
[5] Master student, Youcai Tan, Central South University, No. 932 Lushan South Road, Changsha, China, 1623455719@qq.com

During tunnel operation in karst regions, common issues such as lining cracks and water leakage are frequently observed (Fan et al., 2024). In severe cases, these can escalate into mud inrushes and collapses (Fan et al., 2018). Karst conduits and large faults near tunnel alignments often result in elevated water pressures, sediment accumulation, and large-scale inrushes (Ou et al., 2024).

The direct mechanism underlying such hazards is typically the buildup of external water pressure behind the lining exceeding its load-bearing capacity, ultimately leading to structural damage (Fan et al., 2024). Based on numerical analyses, the internal and external causes of tunnel water-related hazards are identified as the geological conditions of the tunnel zone and extreme weather conditions, respectively.(Ma et al., 2022). For instance, when a tunnel intersects a water-rich fault, excavation disturbance substantially increases the probability of water-related hazards during operation (Peng et al., 2020). Lithology, adverse geological conditions, groundwater level, geomorphology, stratal inclination, lithological contacts, and fissure development have been identified as important indices for hazard risk evaluation (Wang et al., 2016). Similarly, rock solubility, geological structures, surface catchment capacity, and hydrogeological conditions have been highlighted as critical factors in the sudden occurrence of water inflows in karst tunnels (Zhao et al., 2024).

In monsoon climate zones such as Guangdong Province, China, rainfall is highly seasonal, with the majority concentrated in summer. Continuous heavy rainfall provides a substantial source of groundwater recharge (Lyu and Yin, 2023). To address the resulting risks, quantitative groundwater monitoring systems within tunnels have been established, allowing for in situ measurement of pore pressure and drainage to identify potential hydraulic instabilities (Čokorilo Ilić et al., 2019). Improved methods for sensor precision and wireless transmission in complex tunnel environments have been developed, enabling real-time monitoring of water pressure, displacement, and stress (Wang et al., 2021). The acceleration of rainfall infiltration through subsurface seepage pathways further complicates tunnel stability. In karst regions, conduit flow demonstrates both laminar and turbulent regimes. While turbulent flow dominates under high-intensity rainfall, significantly affecting the seepage field, laminar flow largely governs the drainage recession process (Chang et al., 2015). Moreover, increases in conduit diameter within certain ranges enhance the overall drainage capacity of tunnels (Gao et al., 2024).

Despite these advances, a comprehensive understanding of the mechanisms underlying water-related hazards in operational highway tunnels remains limited. The concealed nature of the subsurface environment, coupled with variability in lithology, joint development, and groundwater networks, complicates the study of subsurface seepage pathways and their contributions to hazard development (Gouy et al., 2024; Pardo-Igúzquiza et al., 2012). This challenge is especially pronounced in operational tunnels, where seepage pathways may evolve over time, extending into deeper strata.

Therefore, long-term field monitoring in operational tunnels—particularly through synchronized measurements of rainfall, pore pressure, and drainage—is essential. Such monitoring not only quantifies the lag between surface precipitation and water pressure response within the tunnel, but also provides a means to assess the performance of drainage and waterproofing systems under real operational conditions.

In this study, hydrogeological investigations were carried out in six operational highway tunnels in Guangdong Province, China, and a six-month continuous monitoring program was implemented in a representative tunnel. By capturing and analyzing the rainfall–water pressure–drainage sequence, this study identifies the temporal delay in water pressure response and evaluates the risks posed by hydraulic loads during drainage system failures. Ultimately, the study aims to clarify the complete process from rainfall to hazard occurrence in operational highway tunnels and to summarize the mechanisms underlying these water-related hazards.

2. HYDROGEOLOGICAL INVESTIGATION OF TUNNEL HAZARDS

2.1. Overall Location

The geographical locations of the tunnels investigated for hazards are shown in Figure 1. All six surveyed tunnels are located within Guangdong Province, China (Fig. 1(a)), and are twin-tube separated expressway tunnels. Among them, Chalinding Tunnel, Egongji Tunnel, and Shiyashan Tunnel are situated in the mountainous western region of Guangdong Province, while Dayaoshan No. 1 Tunnel, Dayaoshan No. 3 Tunnel, and Zhongshanding Tunnel are located in the mountainous northern region of Guangdong Province, as shown in Fig. 1(b). Fig. 1(c-e) illustrates the specific location of each tunnel within the district-level administrative divisions. Tunnels ①-③ are situated along the Guangzhou-Kunming Expressway, and Tunnels ④-⑥ are located on the Lechang-Guangzhou Expressway.

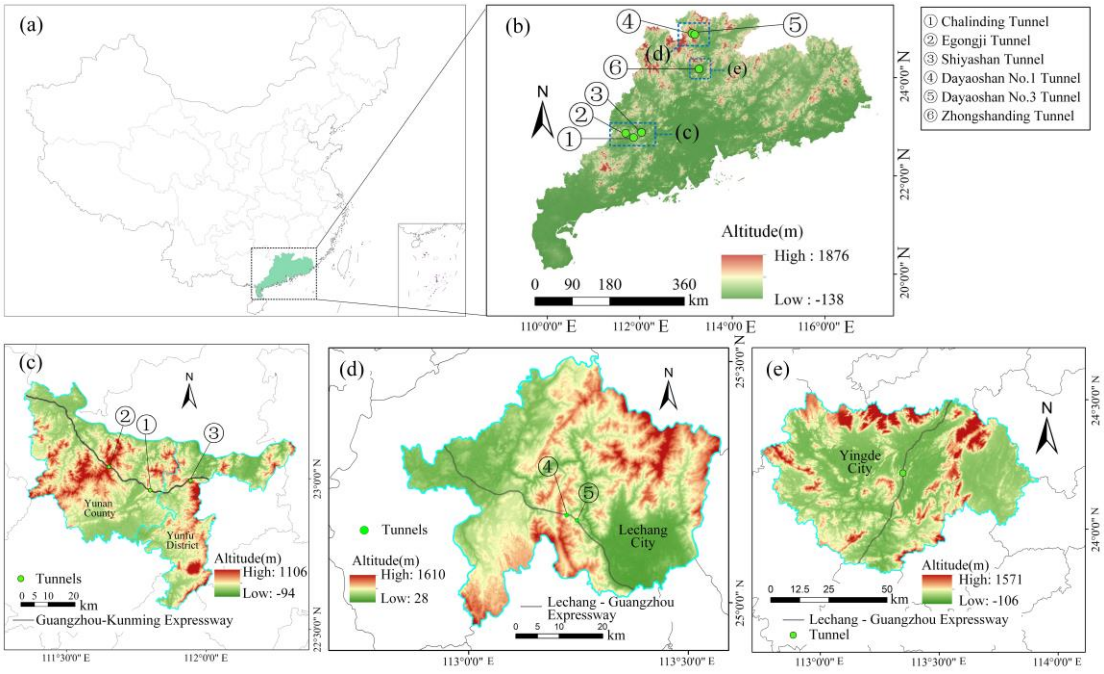

Figure 1. *The geographical location of the investigated tunne*

2.2. Statistical Characteristics of Hazards

The longitudinal geological profiles of the left tubes of Chalinding Tunnel and Dayaoshan No. 1 Tunnel are presented in Fig. 2, with the locations of identified hazards clearly annotated.

In Chalinding Tunnel, several hazard locations were documented. At LK123+959.5–971.5, the sidewall experienced lining bulging and cracking in 2012. The section LK124+392–433 developed a full-length longitudinal crack with a maximum length of 12 m on the sidewall in 2020, an area adjacent to a geophysical anomaly zone. Within LK125+005–050, the drainage ditch suffered a water and mud inrush in 2014. Seismic imaging at this location revealed 23 karst development zones and one structural fracture zone nearby. At LK125+270, the vehicular cross-passage experienced significant water leakage in 2013, followed by recurring drain-hole blockages in 2019, 2021, and 2022. A nearby solution cavity was also identified.

In Dayaoshan No. 1 Tunnel, key hazard-related features were observed. Near the left tube entrance, a solution cavity developed both laterally and vertically. Approximately 20 m into the cavity from the entrance, the invert elevation decreases by about 8 m, and groundwater is present at the bottom. Within a 500 m radius of the entrance, thirteen surface subsidences were recorded, suggesting a potential link to hazards in this area. Near the tunnel's fault zone, joint fissures are highly developed and contain abundant fissure water. On the surface above the tunnel, five major gullies act as runoff channels, and a small reservoir is situated on a hilltop approximately 650 m from the tunnel exit.

The regional topography and contour maps for all six tunnels are shown in Fig. 3. Hazards were consistently observed near gully lines. In Zhongshanding Tunnel, four of five documented hazards were located within karst collapse zones. Fig. 3 further indicates that hazards were significantly less frequent beneath hilltops compared with foothills, where the majority were concentrated.

Based on the hydrogeological investigation across the tunnel group, the characteristics of 36 hazard points were statistically analyzed. This analysis integrated tunnel inspection records, regional elevation maps, and longitudinal profiles. For each hazard point, information was compiled on tunnel burial depth, surrounding rock grade, lithology, hazard manifestation, position within the tunnel, nearby preferential seepage pathways, and corresponding surface topography. These data are summarized in Table 1.

Fig. 4 presents categorized statistics for all hazard characteristics. Regarding burial depth (Fig. 4a), 88.9% of hazards occurred at depths exceeding 50 m, with 12 buried deeper than 150 m. This indicates that the groundwater pressures causing tunnel damage are generally modest (Luo et al., 2024). This distribution pattern, together with the findings in Fig. 4f, suggests a close association with preferential seepage pathways. The statistical results for hazard location within the tunnel (Fig. 4b) show that the majority occurred at the crown (15 cases) and pavement (11 cases), while others were distributed on sidewalls, construction joints, drainage ditches, and cross-passages.

Analysis of lithology and weathering degree (Fig. 4c) revealed sandstone (17 cases) and siltstone (14 cases) as the dominant rock types in hazard zones, while limestone accounted for only 5. Slightly to moderately weathered

rocks were most prevalent. Physical weathering processes such as freeze–thaw cycles, thermal expansion–contraction, excavation unloading, and root wedging fracture the rock and create new fissures, thereby increasing pathways for groundwater flow. Chemical weathering, including carbonate dissolution, increases porosity and generates new pores. Both processes enhance hydraulic conductivity. Although more weathered rocks generally show a higher probability of hazards, the deep burial (>50 m) of most hazard points in this study correlates with less-weathered rock masses compared with near-surface zones (as shown in Fig. 2a). Consequently, hazards in highly weathered rock masses were rare, accounting for only 5.6% of the total.

The statistics for hazard manifestation (Fig. 4d) indicate that crack seepage was the most common phenomenon (50%), followed by water leakage (38.9%). Four severe cases involved structural damage and water/mud inrush. Concerning surrounding rock grade (Fig. 4e), rock masses worse than Grade IV accounted for 80.5% of hazards. Poorer rock quality correlates with fragmentation, porosity, and joint development, all of which increase hazard probability.

Investigation of preferential seepage pathways near hazard points (Fig. 4f) showed that more than half were associated with such pathways. In areas with well-developed joints or fault belts, fractures provide efficient conduits for surface water infiltration. In water-rich and karst terrains, these pathways accelerate the rise of groundwater levels following rainfall, while storage structures maintain locally elevated water pressures.

Finally, the analysis of surface topography above hazard locations (Fig. 4g) revealed that 75% corresponded to catchment structures. Specifically, 8 hazard sites were located beneath depressions, 21 beneath valleys or ravines, and 8 beneath sinkholes, karst collapse depressions, or funnels. Several sites corresponded to more than one converging topographic feature.

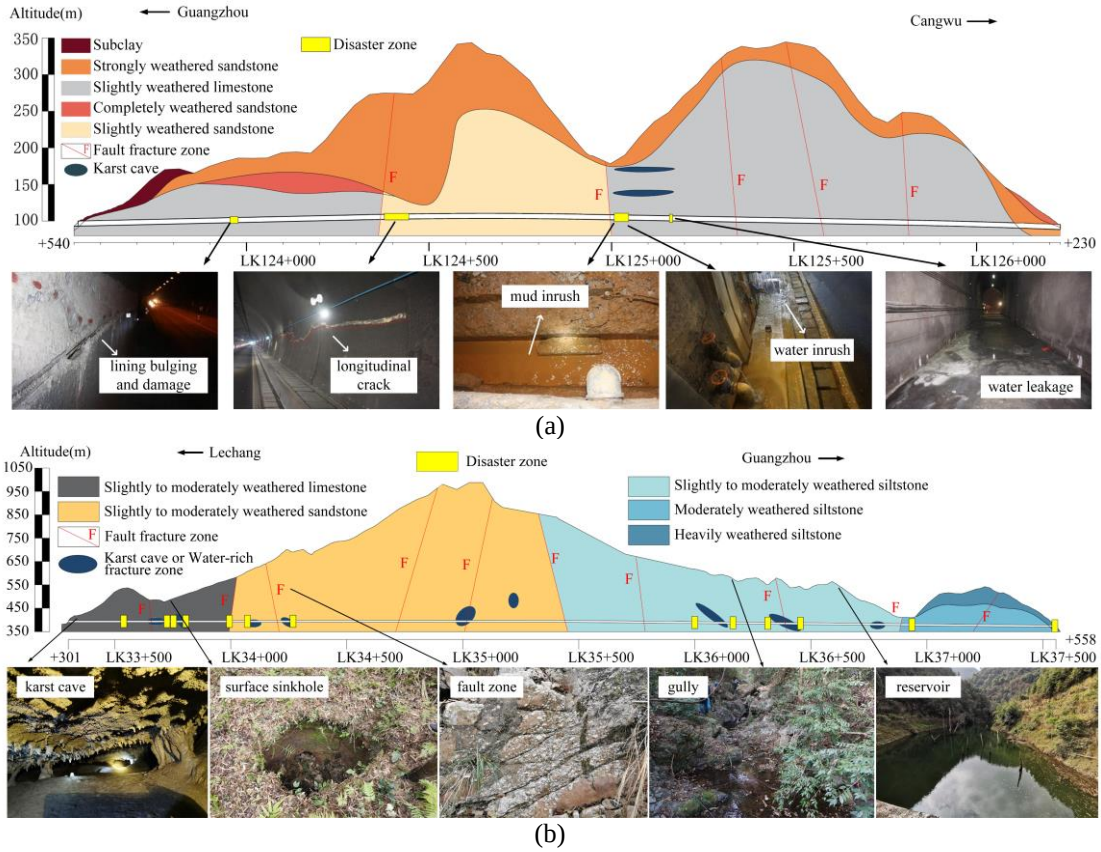

Figure 2. *Geological profile of tunnels. (a) Chalinding Tunnel (left line). (b)Dayaoshan No.1 Tunnel (left line).*

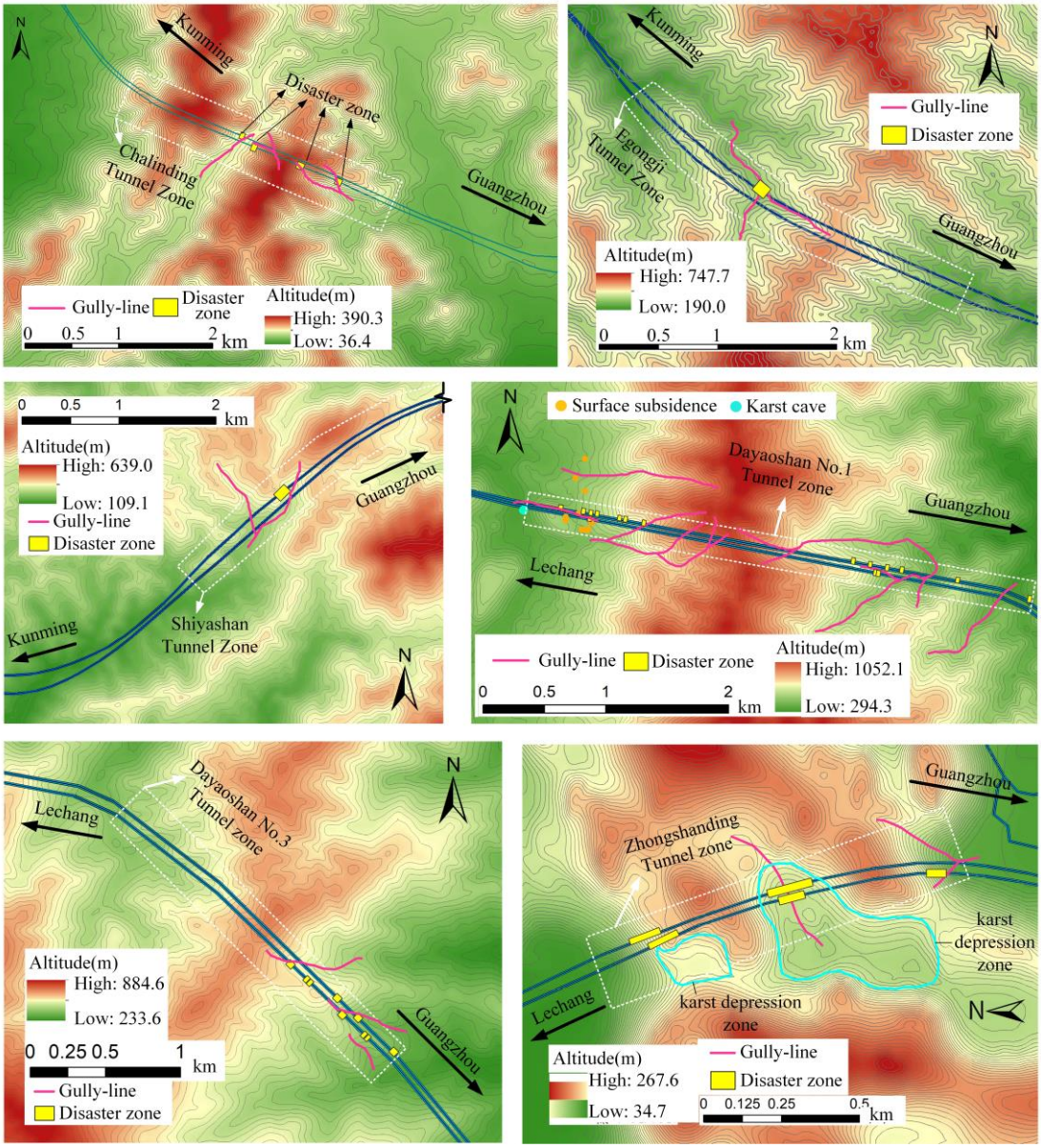

Figure 3. *Tunnel surface topography and contour lines. (a) Chalinding Tunnel. (b) Egongji Tunnel. (c) Shiyashan Tunnel. (d) Dayaoshan No.1 Tunnel. (e) Zhongshanding Tunnel*

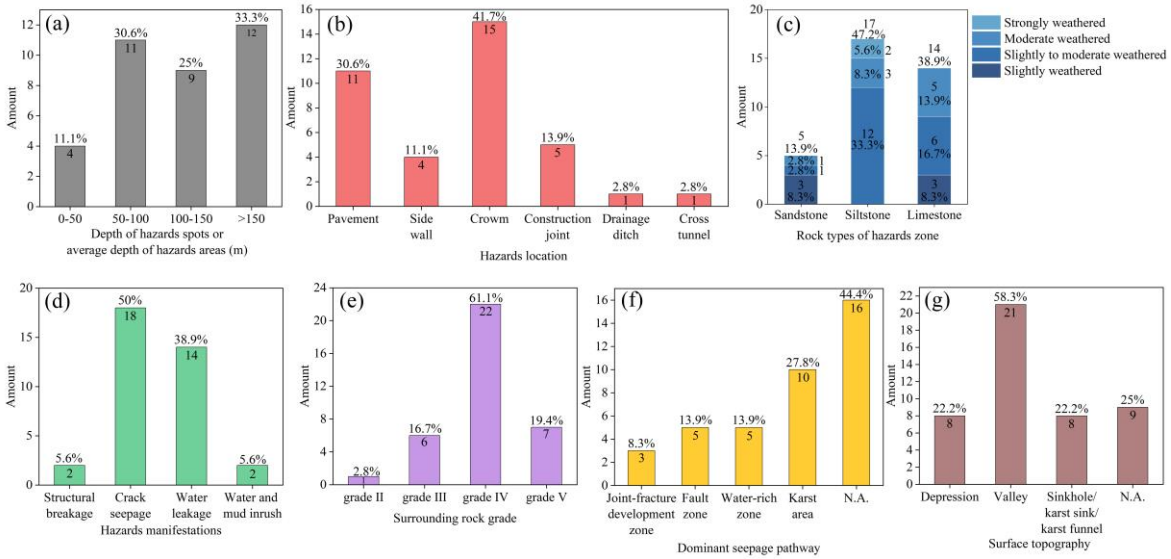

Figure 4. *Statistical results of tunnel water-related hazards characteristics*

3. HYDROLOGICAL MONITORING

3.1. Monitoring Program

All six tunnels investigated in this study are located within a subtropical monsoon climate zone. Under the influence of this climate, rainfall is highly seasonal and concentrated in the summer months. Investigation results show that most tunnel water-related hazards occur between May and September, coinciding with the peak rainfall period. To further analyze the triggering mechanisms of these hazards, a comprehensive hydrological monitoring system was installed at the Dayaoshan No. 1 Tunnel. At the LK36+265 section of the left tube, four piezometers were installed, and one rain gauge was deployed on the ground surface near the tunnel exit. The instrument layout is illustrated in Fig. 5(a).

The configuration of the piezometers is shown in Fig. 5(b). Four vibrating-wire piezometers were installed at specific positions: the overtaking lane side ditch, the overtaking lane sidewall, the slow lane side ditch, and the slow lane sidewall. An automated data acquisition and wireless transmission system was employed to enable continuous monitoring. The installation procedure is illustrated in Fig. 5(c). A borehole approximately 4 cm in diameter and 2.5 m deep was drilled at each designated location. Sand was first placed at the bottom of the hole, followed by the piezometer. The borehole was then backfilled with sand to a depth of approximately 1.2 m, overlain by a 0.7 m thick bentonite layer, and finally sealed with cement mortar grout.

Dayaoshan No. 1 Tunnel adopts a unidirectional drainage slope. The tunnel cross-section and its waterproofing and drainage system are presented in Fig. 6. Circumferential and longitudinal drainage blind pipes were installed outside the tunnel lining, with circumferential pipes spaced at 20 m intervals. Water collected by these pipes was conveyed through transverse pipes into the side ditches and subsequently discharged from the tunnel. The rain gauge, shown in Fig. 5(e), is equipped with a piezoelectric sensor and powered by a solar panel mounted at the top.

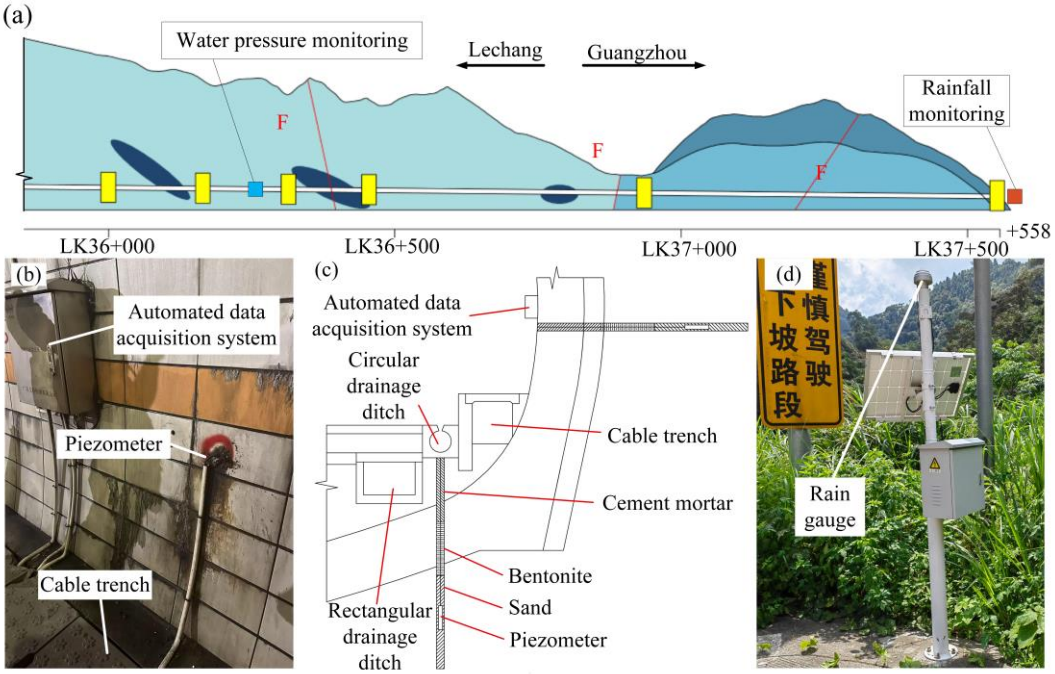

Figure 5. *Instrumentation Layout in Dayaoshan No.1 Tunnel*

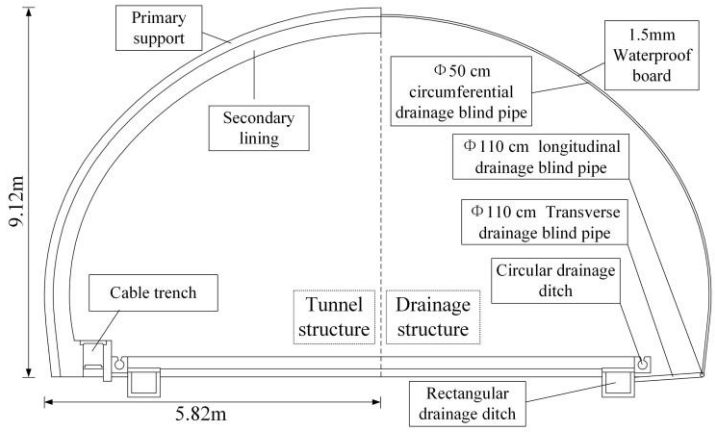

Figure 6. *Tunnel structure and drainage system of Dayaoshan No.1 Tunnel LK36+265*

3.2. Monitoring Results

The Chinese rainfall intensity classification standard defines seven levels of precipitation based on 24-hour cumulative rainfall: drizzle (<0.1 mm), slight rain (0.1–9.9 mm), moderate rain (10.0–24.9 mm), heavy rainfall (25.0–49.9 mm), rainstorm (50.0–99.9 mm), heavy rainstorm (100.0–249.9 mm), and extremely heavy rainstorm (>250 mm). During the six-month monitoring period, a series of intense rainfall events were recorded, including two extremely heavy rainstorms, ten heavy rainstorms, eleven rainstorm events, and twenty heavy rainfall events, as shown in Fig. 7.

A six-month continuous monitoring campaign of rainfall and water pressure in the Dayao Mountain No. 1 Tunnel was conducted from April 1 to September 30, 2024. Figure 7 presents the rainfall–water pressure monitoring results at section LK36+265 of the tunnel. Among the four piezometers installed within this section, the one located on the sidewall of the passing lane failed to provide valid data due to malfunction. Under frequent heavy rainfall conditions, a total of 21 distinct water pressure rise intervals were identified by the remaining three piezometers, each of which was consistently preceded by consecutive rainfall events.The longest continuous water pressure increase occurred at monitoring point ①, located in the side ditch of the slow lane. Following four

consecutive days of rainfall not less than the *Rainstorm* grade and two additional days reaching the *Extremely Heavy Rainstorm* grade, the water pressure began to rise from the fifth day onward. This increase lasted for eight consecutive days, during which the water pressure rose from approximately 0 to 34.2 kPa, yielding a net increment of 32.2 kPa. The largest water pressure increment was recorded at monitoring point ③, located in the side ditch of the passing lane. After three consecutive days of rainfall not less than the *Rainstorm* grade, the water pressure began to increase on the fourth day, reaching a cumulative increment of 58.6 kPa within five days.

Before July 2024, the overall trend at all three monitoring points showed a gradual rise in water pressure. Following rainfall-induced pressure increases, the water pressure decayed slowly. Inspection revealed that drainage pipes in the tunnel were partially clogged. After cleaning and dredging the drainage pipes and ditches in early July, the water pressure began to decrease progressively. These observations indicate a strong correlation between surface rainfall and water pressure increases in the tunnel, with a noticeable lag effect. During extended dry periods, water pressure gradually declined to nearly zero, suggesting that effective tunnel drainage maintained the groundwater level below the tunnel floor. Conversely, during consecutive rainfall events, infiltration from the ground surface recharged the subsurface, raising the surrounding groundwater level and thereby elevating the water pressure around the tunnel, which in turn increased the risk of water-related hazards.

To further characterize the temporal lag in water-pressure response to rainfall, a statistical analysis was conducted on the daily pressure increment within successive days after rainfall events. Because Spearman's rank correlation coefficient (ρ) is a non-parametric measure that captures monotonic (including non-linear) associations between variables (Xue et al., 2023; Yin et al., 2018), it was adopted to quantify the relationship between rainfall and water-pressure changes. For each of the three monitoring locations—slow lane drainage channel, slow lane side wall, and overtaking lane drainage channel—the daily water-pressure change on days 1–7 following rainfall was computed. Rainfall intensity was stratified into four groups: ≥0 mm day^{-1} (all events), ≥10 mm day^{-1} (moderate rain or above), ≥25 mm day^{-1} (heavy rain or above), and ≥50 mm day^{-1} (rainstorm or above). For each rainfall group and each post-event day, Spearman's ρ between daily rainfall h (mm) and the daily water pressure change Δp (kPa) was calculated:

$$\rho = \frac{\sum_{i=1}^{n}\left(R_{h,i}-\bar{R}_h\right)\left(R_{\Delta p,i}-\bar{R}_{\Delta p}\right)}{\sqrt{\sum_{i=1}^{n}\left(R_{h,i}-\bar{R}_h\right)^2}\sqrt{\sum_{i=1}^{n}\left(R_{\Delta p,i}-\bar{R}_{\Delta p}\right)^2}} \tag{1}$$

$$\bar{R}_h = \frac{1}{n}\sum_{i=1}^{n} R_{h,i} \tag{2}$$

$$\bar{R}_{\Delta p} = \frac{1}{n}\sum_{i=1}^{n} R_{\Delta p,i} \tag{3}$$

On the basis of Fig. 8, the lagged influence of rainfall on water pressure does not extend beyond seven days; accordingly, n=7 was adopted.

The distribution of Spearman's ρ across lag days is shown in Fig. 9. For all three locations, the peak Spearman correlation occurs within the ≥10 mm day^{-1} subset. Within this subset, the slow lane drainage channel exhibits its largest ρ on days 6–7; the slow lane side wall peaks on day 3; and the overtaking lane drainage channel peaks on days 3–4. Hence, after rainfall events of at least 10 mm day^{-1}, the most pronounced lag in water-pressure response at these three sites is approximately 6–7 days, 3 days, and 3–4 days, respectively.

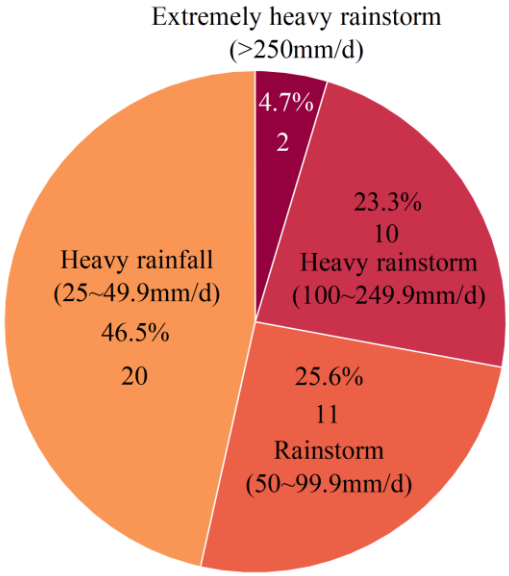

Figure 7. *Rainfall Intensity Distribution*

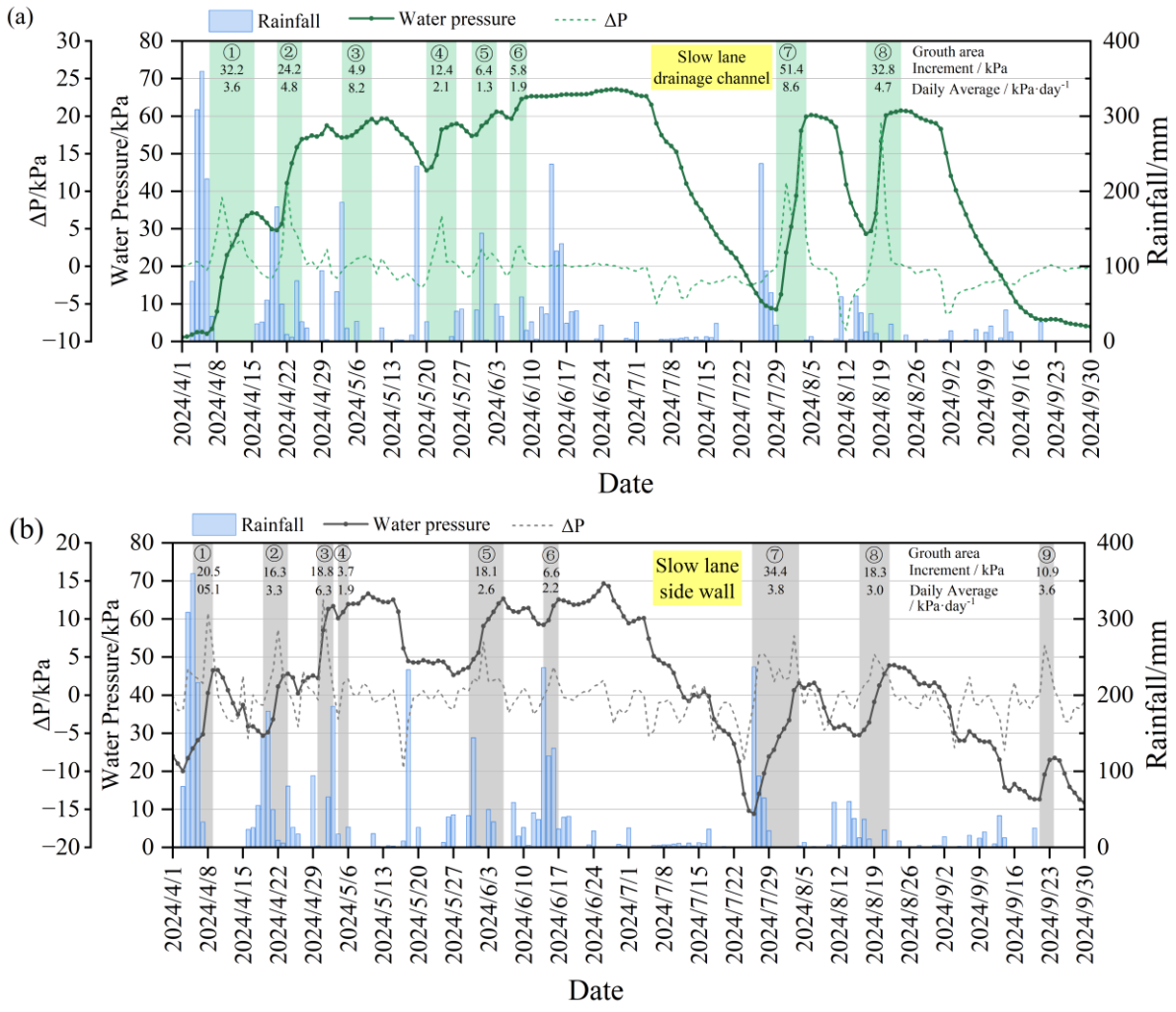

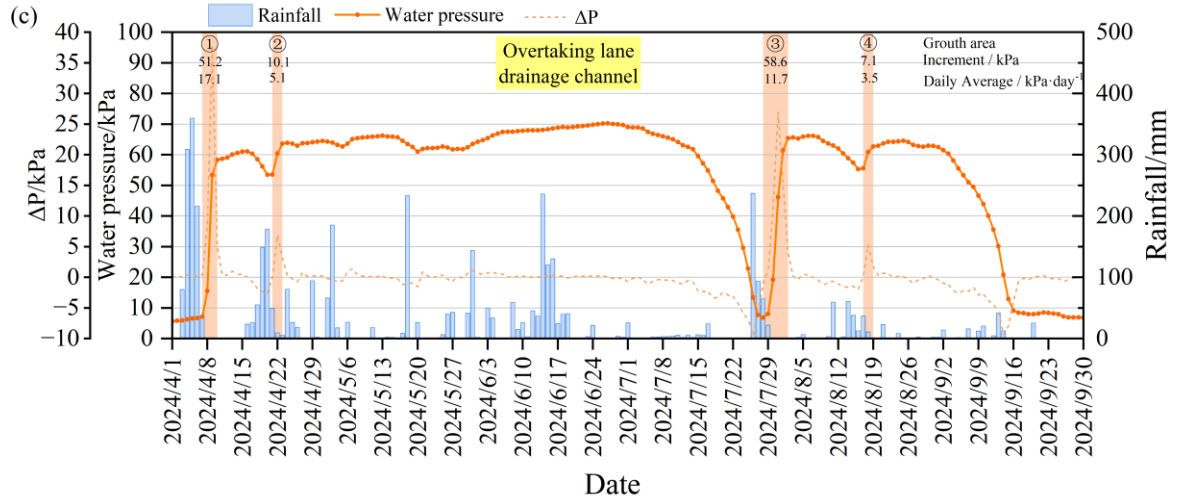

Figure 8. *Rainfall- Water Pressure Monitoring Results. (a) Slow lane drainage channel. (b) Slow lane side wall. (c) Overtaking lane drainage channel.*

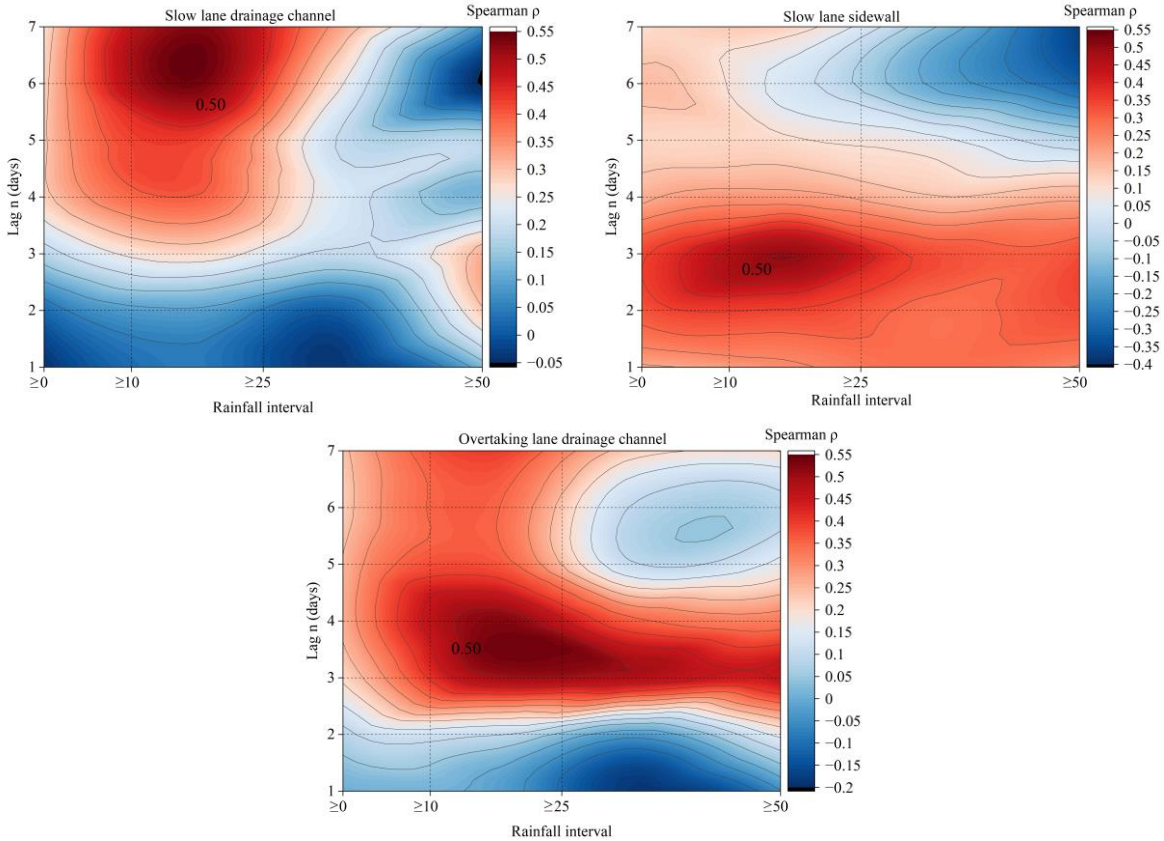

Figure 9. *Time lag distribution of water pressure.*

4. ANALYSIS OF INFLUENCING FACTORS AND DISCUSSION

Based on hydrogeological investigations and monitoring data, the factors and processes contributing to water-related hazards in operational highway tunnels in water-rich areas are summarized in Fig. 10. Under the combined influence of climatic, geological, and drainage conditions, the development of such hazards can be divided into three main stages:

（1）Initial stage:

During this phase, continuous heavy rainfall occurs at the surface, and a significant rise in water pressure typically follows three to five days of persistent torrential rain (Fig. 9). Part of the rainfall infiltrates directly through surface soils and rock layers, while the remainder converges into runoff in valleys and gullies (Fig. 2b).

（2）Infiltration stage:

Rainfall or surface runoff infiltrates through preferential seepage pathways. In karst regions, surface features such as sinkholes or swallow holes may exist. Subsurface carbonate rocks undergo physical and chemical dissolution, forming caves and conduits that connect the surface to the subsurface. These conduits often exceed 10 cm in diameter (Wang et al., 2020), and caves can range from several meters to tens of meters in scale. In non-karst regions with highly weathered rocks (Fig. 4c), strata commonly exhibit well-developed joints and fractures, allowing rainfall to infiltrate as fracture flow into deeper layers. Fault zones function similarly, as tectonic fault planes provide natural underground pathways for surface water infiltration. Surface collapses induced by erosion may also create small depressions or pools, where rainwater either infiltrates or evaporates. Ultimately, surface water accumulates in low-lying areas, forming wetlands or draining into rivers.

（3）Tunnel Impact stage:

In operational highway tunnels, drainage systems are generally designed to discharge infiltrating water completely, thereby maintaining the natural water table below the tunnel level (Fig. 8). However, due to variable forms and rates of seepage, infiltrated water eventually reaches the tunnel vicinity after different durations, leading to a rapid rise in water pressure. If waterproofing and drainage systems perform effectively and the discharge capacity matches the rate of groundwater rise, the water pressure decreases gradually and returns to a stable level. By contrast, if the waterproofing system fails (e.g., due to damaged waterproof boards or clogged drainage pipes caused by sediment or crystallization), or if extreme short-term rainfall combined with preferential pathways (e.g., karst conduits) causes groundwater levels to rise faster than the designed drainage capacity, water pressure around the tunnel remains elevated for extended periods. This sustained high-pressure environment may induce leakage, water and mud inrush, structural cracking, or even failure within a short timespan.

Given the concealed nature of groundwater seepage, numerous research challenges remain. On one hand, detecting subsurface seepage pathways through field investigation or predicting their behavior using stochastic methods can help clarify groundwater flow mechanisms and guide targeted measures for sealing channels and intercepting surface water. This reduces rapid inflow near tunnels and enhances operational safety. On the other hand, under well-characterized hydrogeological conditions, theoretical calculations and numerical simulations can be employed to analyze the rainfall–groundwater seepage–tunnel response process over large regions. Such analyses enable quantification of the complete sequence from rainfall to water pressure increase and subsequent reduction, and help evaluate the impacts of different seepage pathways on operational tunnels. By leveraging quantitative data, the mechanisms of water-related hazards can be investigated in greater depth.

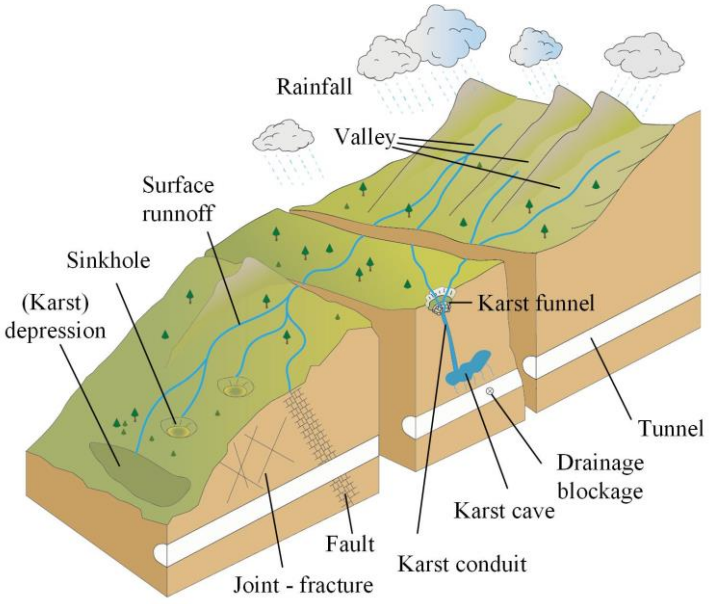

Figure 10. *Progress of Tunnel Hazards*

5. CONCLUSION

(1) Hydrogeological investigations of six operational expressway tunnels revealed that water-related hazards occur most frequently beneath valley lines or topographic depressions. Their occurrence is strongly correlated with surface topography and the presence of subsurface preferential seepage pathways. These hazard-prone locations are typically associated with highly weathered rock, poor surrounding rock conditions, and intensively karstified or water-rich zones.

(2) Monitoring of rainfall and water pressure demonstrated a strong correlation between increases in tunnel water pressure and short-term, continuous heavy rainfall events. The water pressure response to rainfall exhibited a clear time lag, generally exceeding two days, with the lag duration influenced by rainfall intensity, rainfall duration, geological conditions, and drainage capacity. Specifically, for the slow lane drainage channel, slow lane side wall, and vertaking lane drainage channel in this case, the most pronounced lag after rainfall events of ≥10 mm/day was approximately 6–7 days, 3 days, and 3–4 days, respectively.

(3) The formation of tunnel water-related hazards follows a distinct sequence: rainfall infiltration through preferential pathways, the build-up of sustained high water pressure around the tunnel, and subsequent hazard development. Failures of waterproofing and drainage systems were found to significantly amplify the risk of such hazards.

6. ACKNOWLEDGMENTS

This study was supported by the National Natural Science Foundation of China (Grant number 52378422) and Research Project on the Post-Evaluation Methodology System and Key Maintenance Technologies for Highway Tunnel Drainage Systems.

7. BIBLIOGRAPHY

[1] Li, L., Lei, T., Li, S., Zhang, Q., Xu, Z., Shi, S., & Zhou, Z. (2015). Risk assessment of water inrush in karst tunnels and software development. Arabian Journal of Geosciences, 8(4), 1843–1854. https://doi.org/10.1007/s12517-014-1365-3

[2] Wang, X., Li, S., Xu, Z., Li, X., Lin, P., & Lin, C. (2019). An interval risk assessment method and management of water inflow and inrush in course of karst tunnel excavation. Tunnelling and Underground Space Technology, 92, 103033. https://doi.org/10.1016/j.tust.2019.103033

[3] Wu, X., Feng, Z., Yang, S., Qin, Y., Chen, H., & Liu, Y. (2024). Safety risk perception and control of water inrush during tunnel excavation in karst areas: An improved uncertain information fusion method. Automation in Construction, 163, 105421. https://doi.org/10.1016/j.autcon.2024.105421

[4] Li, Z., Chen, Z., He, C., Chen, K., Zhang, H., Ma, C., Li, X., & Liu, M. (2023). Experimental simulation of seepage field distribution for small interval tunnel under varying-head infiltration. Transportation Geotechnics, 41, 101029. https://doi.org/10.1016/j.trgeo.2023.101029

[5] Lin, P., Li, S. C., Xu, Z. H., Wang, J., & Huang, X. (2019). Water Inflow Prediction during Heavy Rain While Tunneling through Karst Fissured Zones. International Journal of Geomechanics, 19(8), 04019093. https://doi.org/10.1061/(ASCE)GM.1943-5622.0001478

[6] Wang, J., Chen, Y., Nie, J., Yan, Z., Zhai, P., & Feng, J. (2022). On the role of anthropogenic warming and wetting in the July 2021 Henan record-shattering rainfall. Science Bulletin, 67(20), 2055–2059. https://doi.org/10.1016/j.scib.2022.09.011

[7] Zhang, S., Song, D., Ye, F., Fu, W., Zhang, B., & Xiao, Q. (2024). Research on flow field characteristics in the karst tunnel face drilling hole (conduit) under the coupling between turbulence and seepage. Tunnelling and Underground Space Technology, 143, 105455. https://doi.org/10.1016/j.tust.2023.105455

[8] Li, S., Xu, Z., Huang, X., Lin, P., Zhao, X., Zhang, Q., Yang, L., Zhang, X., Sun, H., & Pan, D. (2018). Classification, geological identification, hazard mode and typical case studies of hazard-causing structures for water and mud inrush in tunnels. Chinese Journal of Rock Mechanics and Engineering, 5, 1041–1069. https://doi.org/10.13722/j.cnki.jrme.2017.1332 (in Chinese)

[9] Fan, H., Chen, H., Zhao, D., Zhu, Z., Zhao, Z., Zhu, Y., & Gao, X. (2024). Study on lining water pressure distribution and early warning control standard of in-service karst tunnel. Rock and Soil Mechanics, 45(7), 2153–2166. https://doi.org/10.26599/RSM.2024.9436338

[10] Fan, H., Zhang, Y., He, S., Wang, K., Wang, X., & Wang, H. (2018). Hazards and treatment of karst tunneling in Qinling-Daba mountainous area: Overview and lessons learnt from Yichang–Wanzhou railway system. Environmental Earth Sciences, 77(19), 679. https://doi.org/10.1007/s12665-018-7860-1

[11] Ou, X., Ouyang, L., Zheng, X., & Zhang, X. (2024). Hydrogeological analysis and remediation strategies for water inrush hazards in highway karst tunnels. Tunnelling and Underground Space Technology, 152, 105929. https://doi.org/10.1016/j.tust.2024.105929

[12] Ma, Y., Yang, J., Li, L., & Li, Y. (2022). Analysis on ultimate water pressure and treatment measures of tunnels operating in water rich areas based on water hazard investigation. Alexandria Engineering Journal, 61(8), 6581–6589. https://doi.org/10.1016/j.aej.2021.11.040

[13] Peng, Y., Wu, L., Zuo, Q., Chen, C., & Hao, Y. (2020). Risk assessment of water inrush in tunnel through water-rich fault based on AHP-Cloud model. Geomatics, Natural Hazards and Risk, 11(1), 301–317. https://doi.org/10.1080/19475705.2020.1722760

[14] Wang, Y., Yin, X., Jing, H., Liu, R., & Su, H. (2016). A novel cloud model for risk analysis of water inrush in karst tunnels. Environmental Earth Sciences, 75(22), 1450. https://doi.org/10.1007/s12665-016-6260-7

[15] Zhao, R., Zhang, L., Hu, A., Kai, S., & Fan, C. (2024). Risk assessment of karst water inrush in tunnel engineering based on improved game theory and uncertainty measure theory. Scientific Reports, 14(1), 20284. https://doi.org/10.1038/s41598-024-71214-8

[16] Lyu, H.-M., & Yin, Z.-Y. (2023). Flood susceptibility prediction using tree-based machine learning models in the GBA. Sustainable Cities and Society, 97, 104744. https://doi.org/10.1016/j.scs.2023.104744

[17] Čokorilo Ilić, M., Mladenović, A., Ćuk, M., & Jemcov, I. (2019). The Importance of Detailed Groundwater Monitoring for Underground Structure in Karst (Case Study: HPP Pirot, Southeastern Serbia). Water, 11(3), 603. https://doi.org/10.3390/w11030603

[18] Wang, S., Li, L., Cheng, S., Yang, J., Jin, H., Gao, S., & Wen, T. (2021). Study on an improved real-time monitoring and fusion prewarning method for water inrush in tunnels. Tunnelling and Underground Space Technology, 112, 103884. https://doi.org/10.1016/j.tust.2021.103884

[19] Chang, Y., Wu, J., & Liu, L. (2015). Effects of the conduit network on the spring hydrograph of the karst aquifer. Journal of Hydrology, 527, 517–530. https://doi.org/10.1016/j.jhydrol.2015.05.006

[20] Gao, Y., Huang, F., Wang, D. (2024). Evaluating physical controls on conduit flow contribution to spring discharge. Journal of Hydrology 630, 130754. https://doi.org/10.1016/j.jhydrol.2024.130754

[21] Gouy, A., Collon, P., Bailly-Comte, V., Galin, E., Antoine, C., Thebault, B., & Landrein, P. (2024). KarstNSim: A graph-based method for 3D geologically-driven simulation of karst networks. Journal of Hydrology, 632, 130878. https://doi.org/10.1016/j.jhydrol.2024.130878

[22] Pardo-Igúzquiza, E., Dowd, P. A., Xu, C., & Durán-Valsero, J. J. (2012). Stochastic simulation of karst conduit networks. Advances in Water Resources, 35, 141–150. https://doi.org/10.1016/j.advwatres.2011.09.014

[23] Luo, Y., Yang, J., Xie, Y., Fu, J., & Zhang, C. (2024). Investigation on evolution mechanism and treatment of invert damage in operating railway tunnels under heavy rainfall. Bulletin of Engineering Geology and the Environment, 83(5), 160. https://doi.org/10.1007/s10064-024-03655-4

[24] Xue, Y., Zhang, W., Wang, Y., Luo, W., Jia, F., Li, S., & Pang, H. (2023). Serviceability evaluation of highway tunnels based on data mining and machine learning: A case study of continental United States. Tunnelling and Underground Space Technology 142, 105418. https://doi.org/10.1016/j.tust.2023.105418

[25] Yin, M., Jiang, H., Jiang, Y., Sun, Z., & Wu, Q. (2018). Effect of the excavation clearance of an under-crossing shield tunnel on existing shield tunnels. Tunnelling and Underground Space Technology 78, 245–258. https://doi.org/10.1016/j.tust.2018.04.034

[26] Wang, C., Wang, X., Majdalani, S., Guinot, V., & Jourde, H. (2020). Influence of dual conduit structure on solute transport in karst tracer tests: An experimental laboratory study. Journal of Hydrology, 590, 125255. https://doi.org/10.1016/j.jhydrol.2020.125255